Environmental Science Nano

ROYAL SOCIETY OF CHEMISTRY

PAPER

View Article Online
View Journal | View Issue

Cite this: *Environ. Sci.: Nano*, 2025, 12, 894

Are Ni–SiC nanoparticle electroplated coatings a safer alternative to hard chromium? A comprehensive aging, toxicity, and *in silico* study to assess safety by design†

Swaroop Chakraborty, *[a] Nathan Langford,[a] Yvonne Kohl,[b] Dimitra-Danai Varsou,[c] William Stokes,[d] Evangelos Papaioannou,[e] Sascha Wien,[b] Kata Berkesi,[e] Andrew Britton,[d] Bashiru Ibrahim,[a] Antreas Afantitis,[f] Alexandros Zoikis Karathanasis,[e] Andrew Nelson[d] and Eugenia Valsami-Jones *[a]

Considering the increasing interest in utilising nanoparticles (NPs) for advanced, safe, and sustainable coatings, this paper addresses the toxicological concerns associated with nickel–silicon carbide (Ni–SiC) electroplated nanocomposite coatings as an alternative to conventional chromium electrodeposition. We present Ni–SiC nanocomposite coatings as potential substitutes and conduct a comprehensive investigation into the impact of impregnated SiC particles on coating properties. Specifically, we examined the aging of Ni-Watts type and Ni Watts–SiC nanocomposite coatings in various environmental and biological media. Our release and transformation data indicate an enhanced release and transformation of Ni in the simulated media (*e.g.*, up to 200 μg mL^{-1} in cell culture media) and the formation of NiO and $Ni(OH)_2$ species as confirmed by XPS analysis. Transmission electron microscopy data reveal the release of SiC NPs in the respective simulated aging medium. The Ni ion release from Ni-Watts type and Ni–SiC nanocomposite coatings was also investigated *in silico* to support safe-by-design (SbD) approaches in the development of nanoalloys for electroplating. An *in vitro* cytotoxicity assay according to ISO shows a significant reduction in cell viability for Ni–SiC nanocomposite coated samples (up to 80% after 72 hours) compared to standalone Ni-Watts type electroplated coatings (up to 20% after 72 hours). Our findings suggest that the co-deposition of Ni with SiC NPs enhances Ni release, which is a major factor in causing toxicity. These results could be pivotal in the adoption of safe and sustainable by design principles within the electroplating industry. This paper contributes to the fields of nanotoxicology and surface coatings, providing a foundation for designing and optimising environmentally friendly, high-performance coatings with broad industrial applications.

Received 18th August 2024,
Accepted 6th November 2024

DOI: 10.1039/d4en00751d

rsc.li/es-nano

Environmental significance

The environmental significance of this study lies in its critical evaluation of nickel–silicon carbide (Ni–SiC) nanocomposite electroplating as an alternative to traditional chromium electroplating, with a focus on its environmental and biological impacts. While Ni–SiC coatings offer superior mechanical properties, their enhanced Ni ion release in various media, particularly in biological environments, poses significant environmental and health risks. The release of Ni ions and SiC nanoparticles into ecosystems can lead to detrimental effects in living organisms, raising concerns about their long-term environmental persistence and toxicity. This research highlights the importance of adopting safe-by-design (SbD) principles to develop coatings that balance performance with environmental safety. By highlighting the potential ecological hazards of Ni–SiC nanocomposite coatings, the study advocates the development of safer, more sustainable alternatives, contributing to the broader goal of reducing the environmental footprint of the electroplating industry.

[a] *School of Geography, Earth and Environmental Sciences, University of Birmingham, B15 2TT Birmingham, UK. E-mail: s.chakraborty@bham.ac.uk, e.valsamijones@bham.ac.uk*
[b] *Fraunhofer Institute for Biomedical Engineering IBMT, Joseph-von-Fraunhofer-Weg 1, Sulzbach 66280, Germany*
[c] *NovaMechanics MIKE, Piraeus 18545, Greece*
[d] *School of Chemistry, University of Leeds, Leeds LS2 9JT, UK*
[e] *Creative Nano, Metamorfosi, Athens, 14451, Greece*
[f] *NovaMechanics Ltd, Nicosia 1070, Cyprus*

† Electronic supplementary information (ESI) available. See DOI: https://doi.org/10.1039/d4en00751d

1. Introduction

Hard chromium (HC) coatings have dominated the surface finishing industry for almost 100 years due to their excellent hardness (750–1050 HV) as well as wear and corrosion resistance, making them extremely attractive for a series of applications in automotive, aerospace, and other industries.[1] However, the process of acquiring these types of coatings presents significant environmental and occupational health issues as it is based in the use of chromium trioxide (CrO_3) also known as hexavalent chromium (Cr^{6+}), a recognised toxic, carcinogenic and mutagenic compound.[2] The European electroplating industry has undergone notable shifts, particularly concerning environmental issues related to Cr electrodeposition from Cr^{6+}, long used in automotive, aerospace, mining, and petrochemical sectors. EU environmental regulations have prompted exploration into substitute materials and innovative designs to replace Cr electrodeposition while maintaining crucial properties like hardness, friction coefficient, and corrosion resistance.[3,4]

Surface properties of materials are of crucial importance for industrial and commercial applications. It has been proven that surface properties can be improved by means of nanocomposite coatings.[4] In particular, Ni matrix nanocomposite coatings are very promising candidate materials as an alternative to HC coatings due to their potential to achieve excellent wear and corrosion resistance and high hardness, reaching 1100 HV.[5] Nanocomposite coatings, particularly those based on Ni matrices, are emerging as promising replacements for HC coatings due to their ability to achieve similar or superior hardness, wear resistance, and durability. The potential of nanocomposites lies in their tailored structure;[6,7] for instance, lightweight composites made from linear low-density polyethylene (LLDPE) with embedded tungsten (W) particles have shown enhanced radiation shielding properties while maintaining material strength and reduced weight.[8] This example illustrates how the inclusion of nanomaterials, like tungsten nanoparticles, can create multifunctional composites that address specific industrial challenges. Similarly, the superparamagnetic behaviour observed in Ta_2O_5 nanopillars with Ni tips indicates that tailored nanostructures can exhibit distinct magnetic characteristics, which might open additional applications for Ni–SiC coatings in areas like magnetic storage, biomedical imaging, or electronic devices. By evaluating the magnetic response of Ni–SiC coatings, especially under varied thermal conditions, this study could help position these materials as multifunctional, potentially expanding their industrial relevance beyond corrosion and wear resistance.[6,7,9–11]

Simultaneously, among potential alternatives, electrodeposited Ni–SiC nanocomposite coatings have emerged, incorporating ceramic particles for enhanced properties. Addition of hard ceramic NPs, like SiC, into the Ni matrix has demonstrated the ability to boost coating hardness and wear resistance.[5] Additionally, Ni–SiC nanocomposite coatings can possess desirable characteristics in their as-plated state, with SiC reinforcement offering benefits without subsequent heat treatment.[12] These coatings show immense promise in applications where wear resistance and corrosion protection are vital. However, concerns about the potential release of these composite coatings have underscored the necessity for comprehensive safety evaluation.[13]

The release of Ni and SiC NPs from coatings into the environment *via* leachates is concerning, given the status of Ni as a toxic pollutant from anthropogenic sources like mining and industrial waste.[14] Similarly, inorganic NPs and their dissolved species have been identified as emerging contaminants with significant implications for both environmental and human health.[15,16] To assess the potential risks of chemical release, static immersion testing is commonly used. This method, standardised under ISO 10271-2020, evaluates the fouling of materials and the release of chemical leachates from coatings in various simulated media.[17] By characterising the leachates from static immersion cells, our aim was to gain insights into their toxicological potential, informing environmental safety assessments. Assessing cytotoxicity, especially with released Ni and SiC NPs, would be critical to understand the challenges due to their unique properties at the nano level.[9] The overarching aim of this study is to understand the role of NP impregnation in the stability and efficacy of Ni electroplating. We used a comprehensive approach by assessing ageing, toxicity, and *in silico* studies to assess safety by design. Our aim is to understand the stability of standalone Ni-Watts type and Ni–SiC nanocomposite electroplated coatings by performing static immersion testing followed by assessing the transformation and toxicity of leachates. Through a systematic investigation into the influence of SiC particle incorporation on coating characteristics, this research seeks to offer valuable insights for designing and optimising Ni–SiC composite coatings, enabling their widespread application across industries.

2. Experimental section

2.1. Materials

All the chemicals used for conducting the studies were of analytical grade. The salts used to prepare artificial aging media were procured from Sigma Aldrich using the standard composition mentioned in Table S1.† Cell culture media (CCM) were procured from Gibco (Thermofisher, UK). Human lung fibroblasts MRC-5 (CCL-171, LGC Standards GmbH – Germany Office, Wesel, Germany) were cultured using MEM Alpha medium + GlutaMAX (Gibco, cat: 32561 (Thermo-Fisher Scientific/Gibco #32561, Germany)) supplemented with fetal bovine serum SUPERIOR (S0615, Sigma-Aldrich, Darmstadt, Germany) and 100 units per mL penicillin/streptomycin (Thermo-Fisher Scientific/Gibco, #15140, Germany). Cells were cultured in T75 flasks (Greiner

Bio-one, Germany) at 37 °C, 5% CO_2, and 95% relative humidity.

2.2. Fabrication of electroplating coatings

Two distinct coatings were crafted in this study. The initial type comprised pure nickel coatings prepared from a traditional Watts-type electrolyte (Ni-Watts type), serving as the benchmark. The second variant encompassed a nickel-based nanocomposite coating fortified with SiC NPs. Electroplating facilitated the creation of both Ni and Ni–SiC nanocomposite coatings within a lab-scale 1 L electrolyte bath. Brass substrate plates, sized at 3 cm × 5 cm × 0.5 cm (L × H × W), served as cathodes. Meanwhile, a pure Ni-Watts type plate (99.9%) functioned as the anode, positioned at a 10 cm distance from the cathode, maintaining an anode-to-cathode dimension ratio of 1.5.

In the preparation phase, substrates underwent polishing and cleansing with acetone. These samples were selectively masked to enable targeted electroplating within a specific 3 cm × 3 cm active area. Final processing involved rinsing the samples with deionised water (DI), activating them in a 10% v/v HCl solution, and immersing them as cathodes in the electrolyte bath.

Both experimental sets employed a conventional Watts-type electrolytic bath, differing primarily in the composite bath's addition of SiC NPs and SDS surfactant. The SiC NPs, employed for reinforcement, boasted a nominal size of 100 nm. The chemical composition of the electrolytic baths is detailed in Tables 1 and 2. Throughout the study, a pulse current was applied *via* a Metrohm Autolab PGSTAT12 potentiostat/galvanostat electrochemical system.

Concerning electroplating operations in the composite electrolytic bath, a preliminary hour-long ultrasonication treatment ensured homogeneous dispersion of SiC NPs within the electrolyte. High-energy ultrasonication at 200 W, 95% amplitude, and a 50% duty cycle, utilising a 7 mm diameter tip, was employed. Subsequently, the electrolyte was stirred at 400 rpm to sustain NP suspension, with pH adjusted to 3.8 using aqueous NH_3. A stable temperature of 50 °C prevailed throughout the 5 hour electroplating process, yielding approximately 30 μm coating thickness. Post-electroplating, samples underwent DI water rinsing, demasking, ultrasonication bath cleaning, and drying. Contrarily, within the Watts electrolytic bath, direct current was utilized, maintaining pH at 4.4 and a constant 50 °C temperature during the entire 2 hour process, resulting in approximately 30 μm coating thickness.

Table 1 Ni–SiC electrolytic bath composition

Ni/SiC electrolytic bath composition	
Compound	Concentration (g L^{-1})
$NiSO_4 \cdot 6H_2O$	300
$NiCl_2 \cdot 6H_2O$	35
H_3BO_3	40
Saccharin	2
SiC NPs	10
Electroplating conditions	
pH = 3.8	
T = 50 °C	
Pulse current with a 50% duty cycle	
T_{on} = T_{off} = 0.05 s (f = 10 Hz)	
Current density = 2 A dm^{-2}	

Table 2 Traditional Watts electrolytic bath composition

Watts electrolytic bath composition	
Compound	Concentration (g L^{-1})
$NiSO_4 \cdot 6H_2O$	300
$NiCl_2 \cdot 6H_2O$	35
H_3BO_3	40
Saccharin	2
Sodium dodecyl sulfate (SDS)	2.5
Electroplating conditions	
pH = 4.4	
T = 50 °C	
Direct current	
Current density = 2 A dm^{-2}	

The cathodic current efficiency (yield) of the plating process was calculated from the theoretical mass gain of the electrodeposited coating using Faraday's law of electrolysis compared to the actual mass gain of the coatings. The microhardness of the Ni–SiC nanocomposite coatings was determined using a Shimadzu Micro Hardness Tester HMV-G20. The surface morphology and NP distribution in the coating was studied with a TESCAN scanning electron microscope coupled with an energy dispersive X-ray spectrometer (EDS). The scanning electron microscopy (SEM) analysis was conducted using a fixed time mode with a resolution tailored to the specific area of interest. The scan yielded a total count of 1 142 751 with a real time of 125.64 seconds and a live time of 114.827 seconds. The recorded dead time accounted for approximately 8% of the total acquisition time. The SEM was operated at a landing energy of 20 keV. These parameters provided detailed insights into the sample morphology and composition, enabling accurate characterization of the material under investigation. The silicon content of the coating was determined by XRF using a NITON XL5 XRF tester by Thermo Scientific or by SEM-EDS.

2.3. Static immersion aging of Ni-Watts type and Ni–SiC nanocomposite electroplated coatings

The Ni-Watts type and Ni–SiC nanocomposite electroplated coatings as discussed earlier underwent static immersion testing in designated aging cells, as illustrated in Fig. 2. This evaluation was conducted using various environmental and biological simulated media: a 1 mM $NaNO_3$ solution maintained at a neutral pH of 7, synthetic sweat (SS), simulated wastewater (WW), artificial sea water (ASW) and cell culture media (CCM). All the simulated media (shown in

Table S1†) were prepared as per our previously published protocols and standards. For the immersion test, coated samples were placed in the respective aging cells, using a ratio of 1 mL of solution per 1 cm^2 sample surface area as per the static immersion testing ISO standard ISO 10271-2020.[17] These samples were then incubated at room temperature for environmental simulated media (ASW, WW) and 37 °C for biological media (SS and CCM) for periods of 7 days and 3 days, respectively, to simulate aging and study the effects on the material under these controlled conditions.

2.4. Characterisation of leachates post-aging

Leachates from Ni–SiC nanocomposite coated samples, after exposure to various media, were collected from their respective aging cells for analysis to determine the release of specific elements. In the process, 0.5 mL of each leachate sample was subjected to a microwave digestion technique using 0.5 mL of hydrofluoric acid and hydrogen peroxide, with an additional 3.5 mL of nitric acid to bring the volume up to the minimum required for the microwave. This mixture was heated at 180 °C for 30 minutes in a microwave digester to break down the complex sample matrix. Following digestion, the samples were allowed to cool to room temperature and were subjected to elemental analysis using inductively coupled plasma mass spectrometry (ICP-MS). The presence and concentration of Ni and Si in the Ni–SiC nanocomposite coated samples from all the experiments were quantified using ICP-MS. A calibration curve was established to detect levels of Ni and Si ranging from 0.0001 to 1 μg mL^{-1} using ionic standards specific to each element. These measurements were conducted in helium kinetic energy displacement (KED) mode, using specific parameters: a dwell time of 50 ms, 50 sweeps/readings per sample, a helium gas flow rate of 3.5 mL min^{-1}, all managed through Syngistix software.

To investigate the release of SiC NPs from the Ni–SiC nanocomposite coated plates, we performed transmission electron microscopy (80 kV, Jeol 1400, Japan) of the leachates exposed to various media. Further, we also performed X-ray photoelectron spectroscopy (XPS) of the aged Ni-Watts type coated and Ni–SiC nanocomposite electroplated surfaces post-aging to investigate transformation of Ni–SiC nanocomposites upon exposure to various media. Briefly, the media exposed coatings were measured on a SPECS enviroESCA with a Phoibos NAP 150 hemispherical analyser with 1D-DLD detectors and a monochromated 40 W Al K-α (1486.7 eV) X-ray source. The analysed spot size was 0.3 mm in diameter. The plates were secured to the sample holder with conductive carbon tape. Three different spots were measured within the exposed area and one spot measured outside the area for each sample. Surveys were measured at a pass energy of 100 eV and a step size of 1 eV, and high-resolution scans were measured at a pass energy of 50 eV and a step size of 0.1 eV. The findings of these studies were correlated with the leaching and cytotoxicity data to understand the impact of Ni and SiC release from the electroplated surfaces.

2.5. Cytotoxicity assessment of the released leachates

2.5.1. Chemical preparation for *in vitro* studies. Nickel(II) chloride hexahydrate ($NiCl_2{\cdot}6H_2O$) and nickel(II) sulfate hexahydrate ($NiSO_4{\cdot}6H_2O$) as well as a 1 : 1 mixture of $NiCl_2$ and $NiSO_4$ were used in this study as a control to investigate the effect of Ni ions in terms of toxicity. A stock solution (1 mg mL^{-1}) of the Ni containing chemicals was prepared in cell culture media (CCM). *Via* further dilution steps, the following concentrations were prepared in CCM for each chemical: 1000|600|400|200|100|50|25|12.5|6.25 μg mL^{-1}. We also investigated the impact of SiC NPs on cytotoxicity. For SiC NPs, a stock solution of 200 μg mL^{-1} was prepared. The SiC concentrations tested were 100|10|1.0|0.5|0.25|0.125|0.0625|0.03125|0.0156 μg mL^{-1}.

2.5.2. Leachate formation in aging cells. Before leachate formation, the coated samples underwent a sterilisation process. They were treated with 70% ethanol at room temperature for an hour, after which the ethanol was removed and allowed to evaporate. The surface of the aging cells was wiped with 70% ethanol and subjected to UV irradiation at room temperature for an hour within a sterile bench (HeraSafe KSP18, Thermo Fisher Scientific, Germany).

With the coated surface (approximately 3 cm × 3 cm) facing upwards, the sterile Ni–SiC nanocomposites and Ni-Watts type electroplated samples were positioned in the aging cells and coated with 2.0 mL of CCM each. Following extract formation at 37 °C, 5% CO_2, and 90% relative humidity for 24 and 72 hours, the extracts were consolidated per time point and sample type. The extracts from the aging-cells with Ni–SiC electroplated samples at 24 hours, aging-cells with Ni–SiC samples at 72 hours, aging-cells with Ni samples at 24 hours, and aging-cells with Ni samples at 72 hours were combined in a 15 mL tube. Subsequently, the resulting extract underwent cell viability studies and ICP-MS analyses.

2.5.3. Cell viability assay. The cytotoxicity assays, WST-1 and BrdU (Roche, Germany), were conducted in 96-well plates (Greiner Bio-one, Germany) using cells passaged on-site under 20 passages. Cells were seeded at a density of 1×10^4 cells per well and cultured at 37 °C for 24 hours. Subsequently, the CCM was replaced with 100 μL of the test components, including chemicals (refer to the "Chemical preparation for *in vitro* studies" section) and formed extracts (refer to the "Leachate formation in aging cells" section). Alongside these test components, a panel of controls was introduced, encompassing CCM as a reference, 0.4% 2-hydroxyethyl methacrylate (Sigma-Aldrich, Germany) as a positive control, and RM-C (high-density polyethylene film, 3 cm × 10 cm, thickness *ca.* 0.7 mm, lot: C-161, Company) as an ISO 10993 negative control material without cytotoxic effects for extract formation studies.

2.5.4. Metabolic activity assessment *via* the WST-1 assay. The WST-1 assay evaluated cellular metabolic activity by measuring the reduction of tetrazolium salt WST-1 to formazan within the mitochondria of metabolically active/healthy cells. This enzymatic reaction induces a measurable color change in the plate reader. Post 24 hour incubation with the extract, CCM replaced the extract, and 10 μL per well of WST-1 reagent was introduced. After 2 hours, the colorimetric signal, indicative of metabolic activity, was assessed using a plate reader (Infinite F200, Tecan, Waldkirch, Germany) at ex/em wavelengths of 450/690 nm.

2.5.5. Cell proliferation analysis *via* the BrdU assay. The BrdU assay was employed to measure cell proliferation through the incorporation of BrdU (5-bromo-2′-deoxyuridine) into newly synthesised DNA. Cells were first incubated with test extracts for 24 hours. Following this, BrdU labeling was initiated by adding BrdU solution to each well, with cells incubated for an additional 2 hours at 37 °C to allow DNA synthesis and BrdU incorporation. Post-labeling, cells were fixed to immobilise cellular components and then incubated with an anti-BrdU antibody, which specifically binds to the incorporated BrdU within DNA strands. To visualise cell proliferation, a substrate solution was added, producing a colorimetric change proportional to the level of DNA synthesis. The intensity of this colorimetric signal, indicative of cell proliferation, was measured at an absorbance of 450 nm, with a reference wavelength of 690 nm, using a plate reader (Infinite F200, Tecan, Waldkirch, Germany). All steps were conducted according to the manufacturer's instructions to ensure reproducibility and accuracy.

2.5.6. Morphological examination. Post-extract incubation, the cell morphology within the 96-well plates was scrutinised using a phase contrast microscope (IX70, Olympus, Germany).

2.6. Development of predictive models for ion release

To support the safe-by-design approaches in future material development, an *in silico* workflow was developed using data from the release studies performed on materials from the Ni and Ni–SiC composite coatings to generate predictive models. All modelling steps were performed in KNIME using the appropriate KNIME,[18] WEKA, and Enalos+[19] nodes.

2.6.1. Data preparation. To evaluate the long-term stability and transformation of Ni-Watts type and Ni–SiC nanocomposite coatings, a comprehensive ageing study was conducted as discussed in sections 2.3 and 2.4. Using both Watts electrolytic bath composition and those developed by using Ni–SiC nanocomposites, we collected data pertinent to sample preparation and characterisation into an integrated dataset (referenced in the ESI†). Detailed endpoints were established, including the quantification of total Ni ion release in 1 mM $NaNO_3$, SS and CCM, to ascertain the coatings' chemical stability and compositional changes over time.

Ni-ion release, chosen as the target variable for modelling, exhibited a wide range of values (2.08–1026.54 μg mL^{-1}). To address this, the Ni-ion release values were log-transformed and used as the dependent variable (endpoint) in the models. This transformation was crucial for enhancing the interpretability and the robustness of the subsequent statistical analyses, allowing for a more precise assessment of the coatings' stability and the potential toxicological implications of their use. To enhance our analysis, we excluded variables that consisted solely of duplicates, as they provided no valuable information. We then consulted experts to further refine and limit the variables to the following set:

- Sample coating preparation type,
- Thickness,
- Exposure media (1 mM $NaNO_3$, SS, CCM),
- Media pH,
- Zeta potential,
- Time of exposure (days),
- Chemical composition changes (XPS).

As a final step before modelling, the variables were normalised to ensure that they contributed equally to the analysis. Gaussian normalisation was applied, resulting in mean values of 0 and a standard deviation of 1.[20]

2.6.2. Model development. After data preprocessing, data were fed into the modelling scheme where models were trained to predict the samples' log-transformed Ni-ion release using two modelling techniques: the *k*-nearest neighbours (*k*NN) and the XGBoost. In the *k*NN approach, the endpoint of the sample is predicted based on its *k*-nearest neighbours in the data space. The proximity between samples is measured using the Euclidean distance. The endpoint prediction is the weighted average of the endpoint values of the *k* closest neighbours, with each neighbour's weighting factor inversely proportional to its distance from the evaluated sample.[20,21] The XGBoost method (extreme gradient boosting) implements an ensemble machine learning algorithm built from decision tree models. Through an iterative process, trees are added to the ensemble so that the prediction error (loss) of previous models is reduced.[22] Finally, to reduce the individual biases and enhance the overall prediction accuracy, the two models were combined into an averaging scheme to acquire consensus predictions.[22]

2.6.3. Model validation. Following the Organisation for Economic Cooperation and Development (OECD) QSAR model validation standards,[23,24] the models were externally validated using a training set and a test set generated by randomly partitioning the initial dataset in a ratio of 0.70 : 0.30. A stratified approach was considered to retain the distribution of samples exposed to the different media in both sets. The training set was used to adjust the model parameters, whereas the test set was not involved in model development and was used as an external validation set to quantify the performance of the model in real-case scenarios. The Gaussian normalisation function used for the training set was applied to the test set before the external validation phase.

According to the OECD[24] statistical model, validation is essential for evaluating a model's performance. To measure

the model's accuracy, appropriate fitness metrics were used for external validation, to measure how closely the model's predictions match actual values. The statistical criteria used to assess the model performance are presented below.

The mean absolute error (MAE, eqn (1)) and the root mean squared error (RMSE, eqn (2)) were used to assess the accuracy of the models. Using these indices together allows for a comprehensive and thorough validation of prediction accuracy, independent of the distribution level of the training-test endpoint values. Lower MAE and RMSE values indicate more reliable models.

$$\mathrm{MAE} = \frac{1}{N}\sum_{i=1}^{N}\left|y_i - \hat{y}_i\right| \quad (1)$$

$$\mathrm{RMSE} = \sqrt{\frac{1}{N}\sum_{i=1}^{N}\left(y_i - \hat{y}_i\right)^2} \quad (2)$$

where N is the number of samples, and y_i and $\hat{y}_i$ are the actual and predicted endpoint values of the ith sample, respectively.

The quality-of-fit between the predicted and experimental values for the training and test sets was measured using the coefficient of determination (R^2, eqn (3)). Values closer to 1 indicate better-fitting models.

$$R^2 = 1 - \frac{\sum_{i=1}^{N}\left(y_i - \hat{y}_i\right)^2}{\sum_{i=1}^{N}\left(y_i - \bar{y}_i\right)^2} \quad (3)$$

where N is the number of samples, y_i and $\hat{y}_i$ are the actual and predicted endpoint values of the ith sample, respectively, and $\bar{y}$ is the average value of the experimental endpoint values.

To assess the reliability of predictions on new data (external validation), the external explained variance[8,24] was used (Q_{ext}^2, eqn (4)). This metric compares the predictions for the test set samples with their actual endpoint values, with Q_{ext}^2 values closer to 1 indicating models with higher predictive power.

$$Q_{\mathrm{ext}}^2 = 1 - \frac{\sum_{i=1}^{N}\left(y_i - \hat{y}_i\right)^2}{\sum_{i=1}^{N}\left(y_i - \overline{y_{\mathrm{tr}}}\right)^2} \quad (4)$$

where N is the number of test samples, y_i and $\hat{y}_i$, are the actual and predicted endpoint values of the ith test sample, respectively, and $\overline{y_{\mathrm{tr}}}$ is the averaged value of the experimental endpoints of the training set.

Furthermore, the quality-of-fit and the predictive ability of the models were assessed using the statistical criteria of Golbraikh and Tropsha[25,26] (see eqn (SI1)–(SI5), including the Q_{ext}^2, eqn (4)) on the test set (Table S3†).

Finally, we performed the Y-randomisation test[27] to ensure that the models' accuracy was not a coincidental outcome. In this test, the modelling calculations were repeated using the initial matrix of independent variables (descriptors) and shuffled values for the endpoint. In each iteration, a model was developed using the scrambled training set and validated with the original test set. If the statistical metrics (*e.g.*, the MAE) of the produced model were deteriorated, compared to the model built with the actual endpoints, then the original model was considered reliable. If the scrambled data produced higher statistical metrics, an acceptable predictive model could not be produced for both modelling methodologies and the original training set.[28–30]

2.6.4. Applicability domain. To ensure the robustness and reliability of predictive models, especially in accordance with OECD guidelines, it is essential to define the applicability domain (AD). The AD represents the specific subset of the data space where a model can make reliable predictions through interpolation. When the model encounters data points outside this designated domain, these predictions should be flagged as unreliable due to the greater uncertainty inherent in extrapolation.[24]

In this study, similarity measurements based on the Euclidean distance among all training and test samples were used to define the AD of the final model. The distance of a test sample to its nearest neighbour in the training set was compared to the predefined threshold (thr, eqn (5)). In the case where this distance for the test sample exceeded the AD limit, its prediction was considered unreliable. The assessment of the AD of the proposed model was performed in our KNIME workflow, using the Enalos+ Domain–APD node that executes the above procedure.[31] The above procedure can be followed for each query sample, when the model is used to assess the ion release of untested samples.

$$\mathrm{thr} = d + Z\sigma \quad (5)$$

where d is the average of all distances included in the subset of distances which are lower than the mean distance value of all training NMs, σ is the standard deviation of all distances included in the subset of distances that are lower than the distance mean value, and Z is an empirical cut-off value (in this case, it was set equal to 0.5).

2.7. Statistical analysis

The aging studies in various biological and environmental media were performed in triplicate (n = 3) and the data of elemental concentration were measured in mean ± standard deviation. The mean values of the coatings comprised testing of three individual coating samples and encompassed three independent experiments. Each extract was evaluated in six wells per 96-well plate (six technical replicates) across three independent experiments. Reference control cells incubated solely with CCM were designated as 100%, defining the influence of extracts as relative values.

3. Results and discussion

3.1. Characterisation of electroplated coatings

Ni-Watts type and Ni–SiC nanocomposite coatings were studied for their performances during plating. As demonstrated in Fig. 1A, we observe a higher yield (~99%) in the samples plated with the Ni Watts type, while lower yields of the order of 95% in the Watts type with the addition of NPs (SiC). All samples had high plating yields which is typical of nickel-plating using Watts baths. The lower performance of baths with NPs is mainly due to the dispersion formed by their presence in the bath. A very important property in the field of plating is the measurement of the hardness of the plated sample. The hardness of the samples was measured and something that is common in the literature was observed, namely the increase in hardness with the use of SiC NPs in the solutions. The metallised samples with the absence of SiC had a hardness of 546 HV while those with SiC had 752 HV (see Fig. 1A, red columns).

Based on the SEM images depicted in Fig. 1B, the magnification seen in the images at 50 μm reveals that the samples containing SiC NPs exhibit a rougher surface compared to the samples without SiC, which appear smoother. This is likely attributed to the adhesion of NPs on the surface, promoting the surface irregularities. The silicon content of the Ni–SiC nanocomposite coating electrodeposited from the Ni-Watts/SiC electrolyte was also measured by XRF, which resulted in 1 w/w% Si-content in the Ni–SiC nanocomposite. The deposit was also measured by EDS for silicon content and the results demonstrated in Fig. S1† complemented and aligned with the XRF results. The energy-dispersive X-ray spectroscopy (EDS) analysis revealed the elemental composition of the sample. The electroplated surface contained Ni predominantly, *i.e.*, 97.50% atomic percentage and 98.79% weight percentage. Si was also present in the sample, although in a lower amount, accounting for 2.50% atomic percentage and 1.21% weight percentage (Fig. S1†). These results provide crucial information about the sample's elemental makeup, confirming the high concentration of Ni and the presence of Si as a minor constituent.

3.2. Transformation of Ni post-aging in various media

Ni Watts type and Ni–SiC nanocomposite electroplated substrates were exposed to various environmental (1 mM $NaNO_3$, ASW, WW) and biological media (SS, CCM) for static immersion testing and aging studies. Post-exposure, both the coated substrates and the medium leachates were analysed using a range of analytical techniques. The pictographic representation showed significant variations in the appearance of the coated areas exposed to different media. Compared to the Ni Watts type coating (Fig. 2A), the Ni–SiC nanocomposite coating exhibited greater degradation in the media. These findings align with the Ni and Si release observed in the respective media. ICP-MS analysis indicated a relatively low release of Ni (6–9 μg mL^{-1} across all samples) in the 1 mM $NaNO_3$ solution (pH 7) over a 7 day aging period, as shown in Fig. 2B. Visually, the coatings appeared undisturbed after this period (Fig. 2A), corroborating the low Ni release levels shown in Fig. 2A and C.

In stark contrast, Ni release was significantly higher in the CCM and SS media, especially after just 3 days and 5 days, respectively, for both Ni Watts type and Ni–SiC nanocomposite electroplated coatings. For the Ni Watts electroplated coating, Ni release in CCM and SS was 64.5 ± 5.9 μg mL^{-1} and 81.3 ± 9.3 μg mL^{-1}, respectively. However, Ni release was even higher in Ni–SiC electroplated coatings in CCM and SS, reaching 148.14 ± 3 μg mL^{-1} and 108 ± 2 μg mL^{-1}, respectively. Visually, the coatings showed significant changes after aging in these biological media (Fig. 2A and C), indicating material degradation, release, or transformation. To prevent bacterial contamination, the aging duration in CCM was limited to 3 days, though longer exposure would likely result in even greater Ni release. This pattern of enhanced Ni release in CCM aligns with the toxicity findings (Fig. 4B), which reported significant toxicity of Ni–SiC nanocomposite samples to MRC-5 cells compared to standalone Ni Watts type electroplated coatings. Each sample

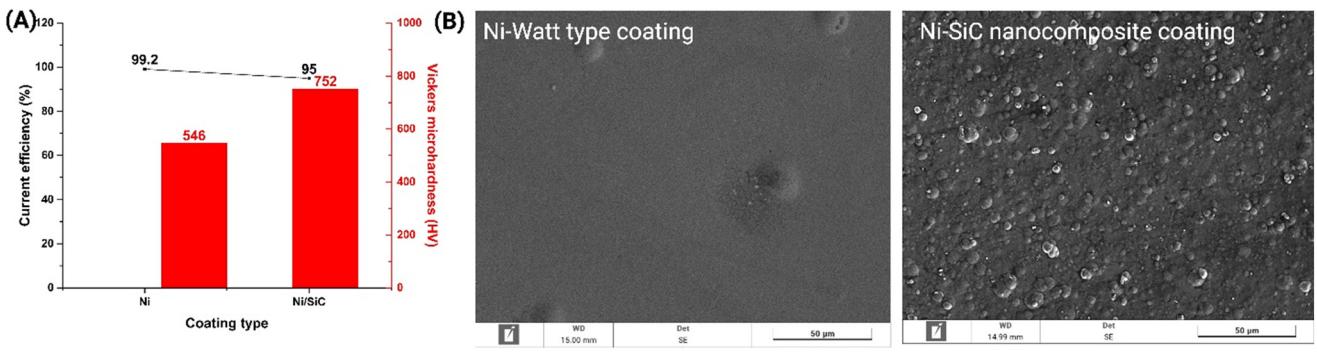

Fig. 1 Characterisation of Ni-Watts type electroplated coatings and Ni–SiC nanocomposite coatings. (A) Cathodic current efficiencies (line & symbol) and Vickers microhardness (column) of coatings deposited from the Ni-Watts type bath (Ni) and Ni–SiC bath (Ni–SiC). (B) SEM images, left: Ni-Watts type coating and right: Ni–SiC-nanocomposite coating (scale – 50 μm).

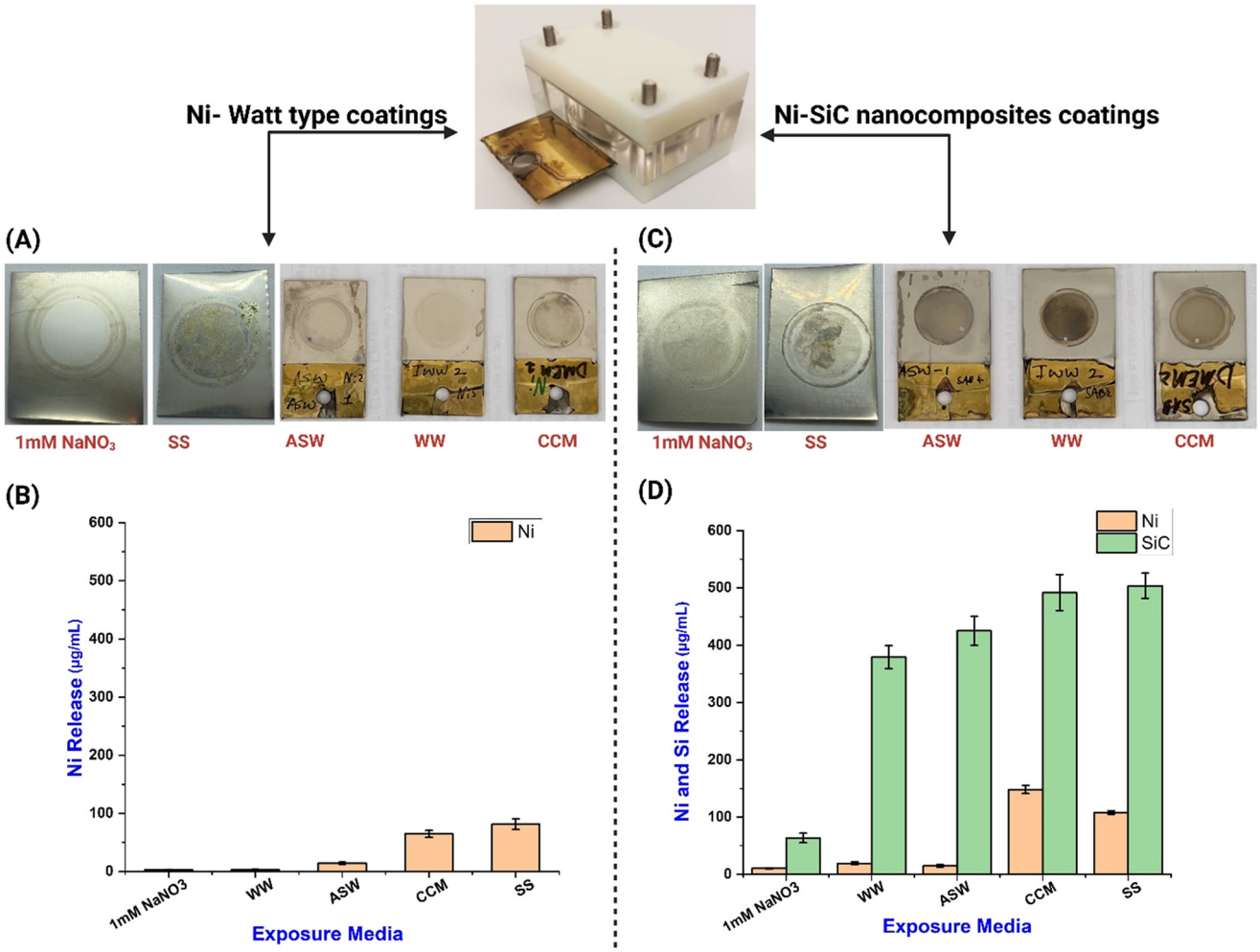

Fig. 2 Characterisation of Ni Watts type and Ni–SiC nanocomposite electroplated coated substrate aging in artificial sea water (ASW), wastewater (WW), cell culture media (CCM), synthetic sweat (SS), and 1 mM $NaNO_3$. Pictographic representation of Ni electroplated samples (A) post-aging in various media and their Ni release profile measured using ICP-MS (B), (C) pictographic representation of Ni–SiC electroplated samples post-aging in various media and their Ni and SiC release profile (D) measured using ICP-MS. The experiments were performed in triplicate (n = 3). The limit of detection (LOD) for Ni is 0.58 ng mL^{-1} and that for Si is 2.18 ng mL^{-1}.

demonstrated Ni release, underscoring the potential toxicological impacts on cellular health.

Fig. 2B and D compare the release profiles of Ni from standalone Ni coatings with and without SiC NPs. The data indicate that coatings with SiC exhibited a higher Ni release rate compared to the Ni Watts type coatings. For instance, Ni release in CCM from the standalone Watts type Ni coating and Ni–SiC nanocomposite coating was 64.5 ± 5.9 µg mL^{-1} and 148.14 ± 3 µg mL^{-1}, respectively. Similar observations were noted across various media, indicating a higher Ni release from Ni–SiC nanocomposite electroplated coatings. This increased release is likely due to the Ni being loosely bound to the SiC NPs, resulting in both Ni and SiC NPs being released into the respective media. Interestingly, Ni release was also observed in environmental media such as WW and ASW in both Ni Watts type and Ni–SiC nanocomposite coatings. Although the Ni release in these simulated environmental media was relatively lower, it was 14.4 ± 2 µg mL^{-1} and 19.4 ± 2.2 µg mL^{-1} in ASW and WW, respectively, for Ni–SiC nanocomposite coatings, and 14.1 ± 1.7 µg mL^{-1} and 3.4 ± 0.3 µg mL^{-1} for Ni Watts type coatings (Fig. 2B and D). The increased release of Ni from both types of electroplated surfaces in biological media can be attributed to the presence of oxidising groups and weak acids in SS and CCM, which facilitate metal ion dissolution.[12,17] This phenomenon is well-documented in the literature, where acidic environments and biological fluids have been shown to enhance the degradation and release of metal ions from coatings.[32] Such interactions highlight the critical role of environmental conditions in the behaviour and stability of electroplated coatings in biological applications.

Additionally, TEM images (Fig. 3A) captured post-aging experiments show the dispersal of SiC NPs in the aging media. The extent of NP release varied across different media, being most pronounced in CCM, followed by WW, and least in ASW. This pattern aligns with the ICP-MS measurements of Si and Ni release across the samples (Fig. 2D), confirming the observed trends in SiC NP and Ni

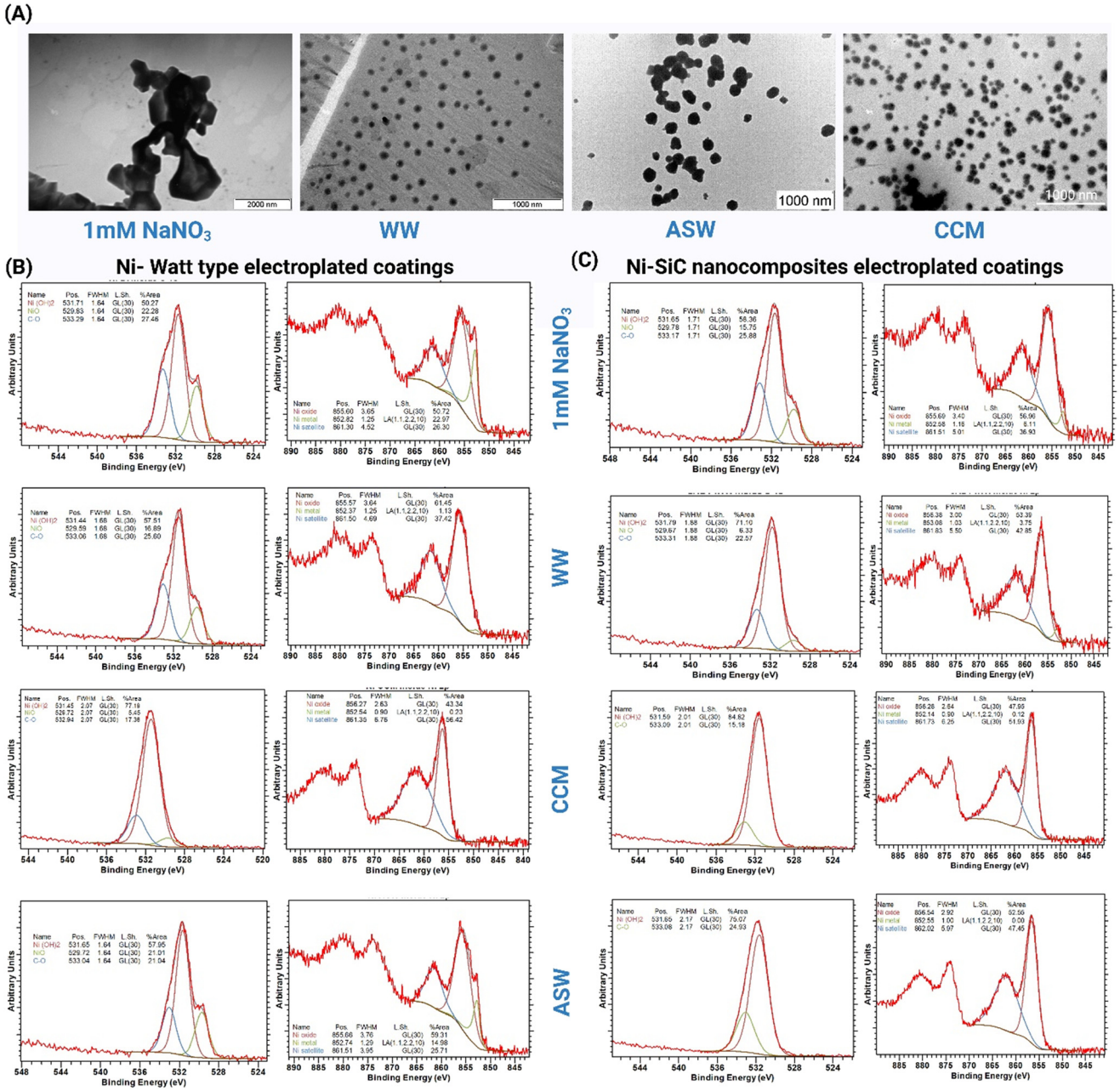

Fig. 3 Characterisation of Ni Watt type and Ni–SiC nanocomposite electroplated coating post aging in various media. (A) TEM analysis of Ni–SiC electroplated aging in artificial sea water (ASW), wastewater (WW), cell culture media (CCM), and 1 mM $NaNO_3$. XPS analysis of Ni-Watts type coatings (B) and Ni–SiC (C) nanocomposite coatings in various simulated media showing transformation of Ni in various media. The chemical composition and respective peaks for Ni and O are shown in the graphs.

metal release. This observed increase in Ni release from coatings with SiC NPs could be attributed to the high surface-to-volume ratio of the NPs, which may loosely capture Ni ions on their surfaces. These ions are then likely released into the aging medium through a diffusion process. As a result, the presence of SiC NPs facilitates a higher level of Ni release into the media compared to coatings that do not incorporate SiC NPs.

XPS spectra (Fig. 3B and C) were analysed and peaks were fitted using casaXPS software.[33] The binding energy was calibrated to the assigned carbon aliphatic peak (C–C) in the C 1s spectra at 284.8 eV. For the C 1s and O 1s spectra, the fitted peaks were constrained to the same FWHM and the line shape for all peaks was kept as GL. The binding energy positions were allowed to float within constraints. The Ni 2p spectra can be more complex to fit due to the presence of satellite features creating multiple peaks for each chemical environment.[34] A simplified fit was modelled whereby the asymmetric metal peak LA (1.1, 2.2, 10) was used in combination with a symmetric mixed oxide/hydroxide peak and a mixed satellite peak (both GL (30)). The primary purpose was to distinguish between

metallic nickel and non-metallic nickel compounds with the lower binding energy of the primary metal peak at 852.5–853 eV being resolvable from the primary hydroxide/oxide peaks at 855.5–856.5 eV and the mixed satellite peaks found at around 860–862 eV. The O 1s spectra can instead be used to distinguish between nickel oxide and nickel hydroxide states with binding energies of around 529.5–529.8 eV and 531.4–531.8 eV, respectively.[35] An organic carbon–oxygen peak sits at around 533 eV and the amount matches to a good approximation with the observed C–O states in the C 1s spectra. In summary, the released Ni underwent transformation into NiO and $Ni(OH)_2$ on the surface of the Ni substrate, as evidenced by XPS analysis. While the specific forms of Ni species in the aging media were not directly assessed, it can be inferred from XPS data that the released Ni likely existed in oxide, hydroxide, and other chemical forms. In contrast, the SiC NPs maintained their chemical integrity and didn't show any transformation in their chemical identity. This stability can be attributed to the high solvation energy and low dissolution tendency of SiC NPs in both biological and environmental media, a phenomenon supported by the existing literature on nanoparticle behaviour in various media.

3.3. Cytotoxicity studies

In adherence to ISO 10993-part 5 (DIN EN ISO 10993-5:2009-10), the biocompatibility assessment of the Ni–SiC nanocomposite and Ni Watts type coatings was conducted in comparison with the raw materials of the coatings ($NiCl_2$, $NiSO_4$, SiC NPs). The leachates from the Ni Watts type and Ni–SiC nanocomposite coatings were formulated within aging cells by introducing CCM onto the defined areas of the coated samples (Fig. 4A). Subsequent evaluation at 24 and 72 hours involved WST1 and BrdU assays (Fig. 4B). As expected, the reference control (CCM), negative control (RM-C), and positive control (HEMA) exhibited the anticipated responses. The Ni–SiC nanocomposite coating notably induced significant and substantial inhibition of metabolic activity, showcasing a decline to 29.2 ± 1.8% after 24 hours and 19.1 ± 0.7% after 72 hours as compared to untreated MRC-5 cells. A time-dependent impact was evident, with a more significant reduction in cell viability observed after 72 h of exposure to

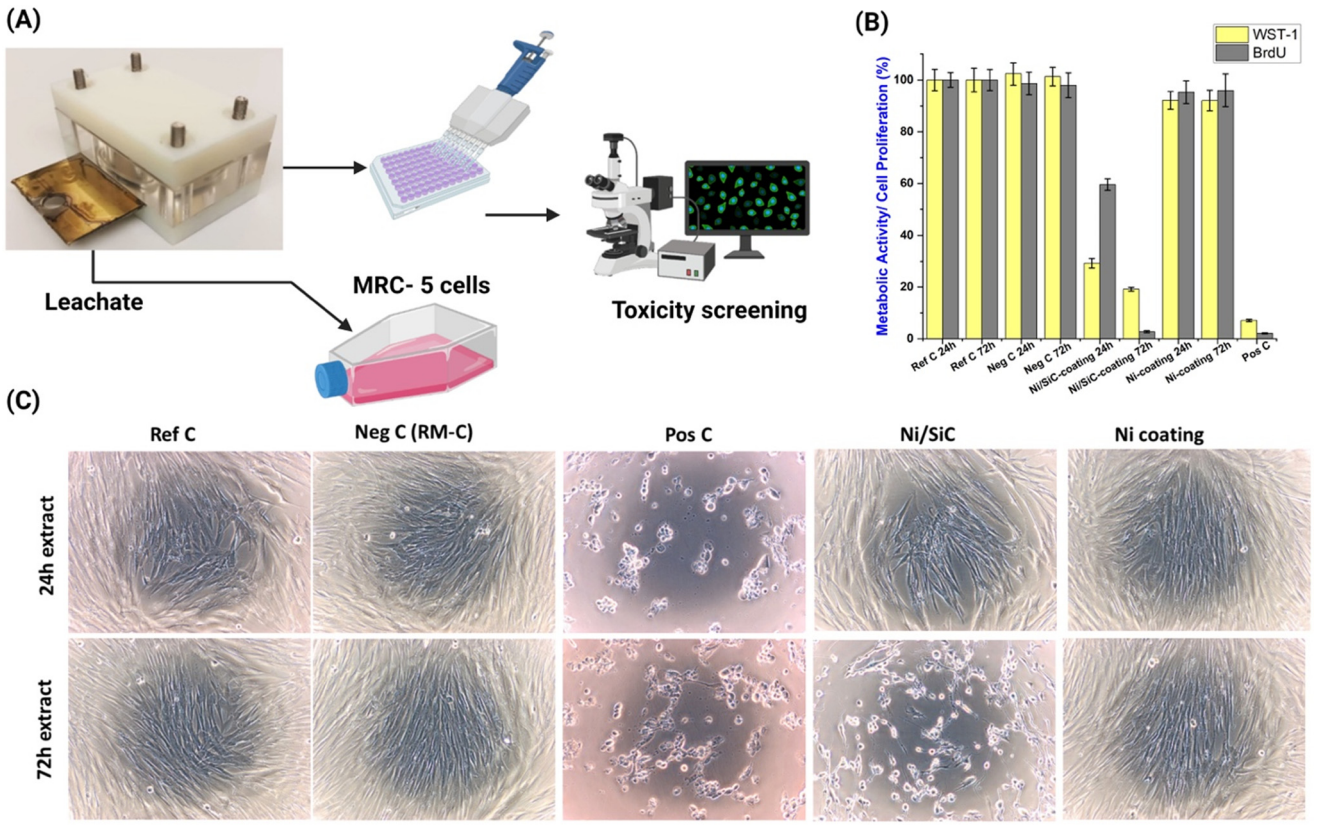

Fig. 4 Cytotoxicity profiling of leachates from Ni Watts type and Ni–SiC nanocomposite electroplated coatings. (A) Schematic showing the aging of Ni and Ni/SiC NP electroplated coatings with CCM and subsequent cytotoxicity assessment on the MRC-5 cell line. (B) Metabolic activity and proliferation rate of human lung fibroblasts (MRC-5) after 24 h and 72 h incubation of the leachates formed on the sample coating using WST-1 and BrdU assays. Reference control: cells cultured in a 96 well plate with CCM; negative control: high density polyethylene film; positive control: hydroxyethylmethacrylate; data of n = 3 are presented as mean ± SD. (C) Microscopic evaluation of MRC-5 cells upon exposure to leachates extracted after 24 hours and 72 hours of aging, negative control: high density polyethylene film; positive control: hydroxyethylmethacrylate; scale bar 200 μm.

leachates. As per the ISO 10993 definition, any inhibition of metabolic activity (formazan formation) exceeding 30% is classified as a cytotoxic effect.[36]

Conversely, the Ni coating did not result in any significant inhibition of metabolic activity. At both 24 and 72 hours, cellular metabolic activity remained within the range of 92%. Correspondingly, regarding cell proliferation, the observations aligned with the outcomes of the WST-1 assay. The proliferation rate was noted at 59.6 ± 2.2% after 24 hours and sharply decreased to 2.7 ± 0.4% after 72 hours (Fig. 4B). Microscopic examination (Fig. 4C) corroborated these findings, revealing distinct alterations in the cellular morphology subsequent to Ni–SiC nanocomposite coating extract incubation with MRC-5 cells. Cells exhibited rounding, loss of adhesion, and eventual detachment (Fig. 4C). These outcomes collectively underscore the distinct effects of Ni–SiC nanocomposite and Ni Watts type coatings on both metabolic activity and cell proliferation, aligning with ISO 10993 guidelines for cytotoxicity assessment.[36–39] The heightened cytotoxic response from the Ni/SiC NP coated extract is in agreement with the Ni and SiC release profile as shown in Fig. 2B and D. There was a clear indication of higher Ni release in the case of Ni/SiC electroplated coatings as compared to that of standalone Ni coatings. By ICP-MS,

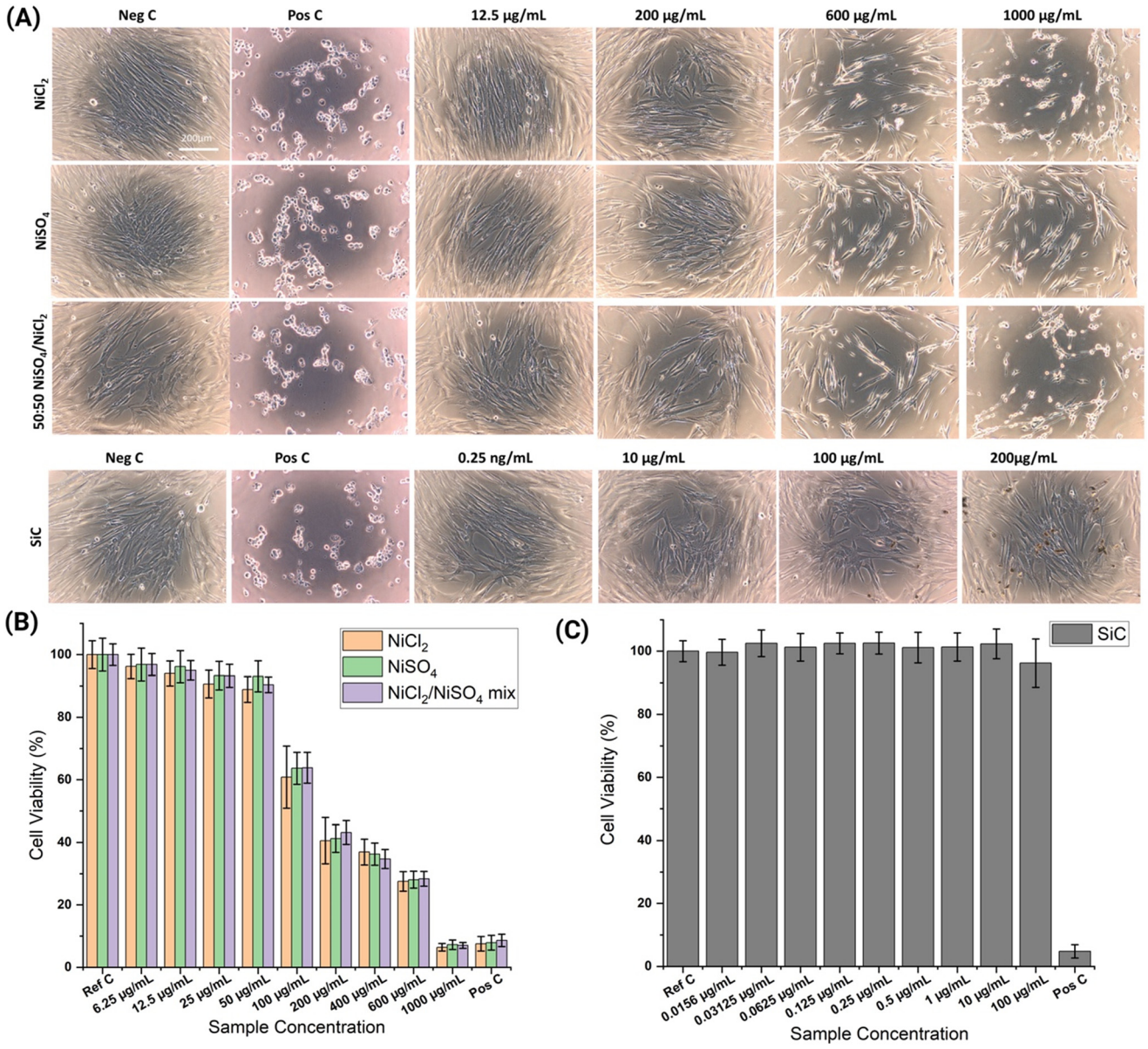

Fig. 5 Cytotoxicity studies on Ni and SiC NPs on the MRC-5 cell line. (A) Microscopy images of human lung fibroblasts (MRC-5) after 24 hours and 72 hours incubation of the extract formed on the sample coating. Negative control: high density polyethylene film; positive control: hydroxyethylmethacrylate; scale bar 200 µm, (B) WST-1 cell viability assay performed on MRC-5 cells with various exposure concentrations of Ni salts showing a concentration dependent cytotoxic effect, and (C) WST-1 cell viability assay performed on MRC-5 cells upon exposure to SiC NPs at various concentrations. The study did not show any significant reduction in cell viability up to a very high exposure concentration.

measurements of the formed extract were performed to identify the specific amount of Ni and Si released during the leachate formation (Table S2†). It is well-established in the literature that Ni ions exhibit significant cytotoxicity, which is likely responsible for the majority of observed cytotoxic responses.[40] This toxicity is due to not only the presence of free Ni ions but also their transformed chemical forms, such as NiO and $Ni(OH)_2$, and various Ni–organic complexes that form in CCM. These transformed species can interfere with cellular processes, leading to oxidative stress and DNA damage, as documented in numerous studies. Furthermore, the interaction of Ni ions with proteins and other cellular components can disrupt normal cellular function, exacerbating cytotoxic effects. A comprehensive understanding of these mechanisms is crucial for evaluating the safety of Ni-containing coatings.

Based on this finding, the concentration of the tested raw materials was defined. The objective of this is to investigate if the cytotoxic responses predominantly occur due to released Ni ions or the combinatorial effect of both Ni and SiC NPs. For all three Ni-components ($NiCl_2$, $NiSO_4$ and a $NiCl_2$/$NiSO_4$ 1 : 1 mixture), after 24 hours exposure a dose-dependent increase in metabolic activity was detected (Fig. 5B). Similarly, the WST-1 cytotoxicity assay was performed on MRC-5 cells after they were exposed to a range of concentrations of SiC NPs (0.0156–100 μg mL^{-1}). Interestingly, both spectrometric and microscopic data suggest that SiC NPs are not cytotoxic to MRC-5 cells even at a very high exposure concentration (Fig. 5C). This observation is in agreement with various research articles demonstrating SiC NPs as non-cytotoxic even at a very high exposure concentration.[41–45] No differences between the effect intensities could be verified. To confirm the impact of Ni on the morphological changes of MRC-5 cells, we performed microscopy imaging, which validates the findings of cell cytotoxicity upon exposure to Ni ions (Fig. 5A).

3.4. Model development and validation

To support the assessment of the ion release and the NP degradation, a computational workflow was developed. Data of the different coating preparation methods (Ni-Watts type and Ni–SiC nanocomposite coatings) were combined with the ageing condition data, the generated data from the post-aging characterisation of the Ni Watts and Ni–SiC nanocomposite surfaces using XPS, and the Ni-ion release measurements from ICP-MS creating a coherent dataset (see the ESI†). After the data pre-processing stage (see section 2.6), the variables selected to develop the predictive model for the log-transformed Ni-ion release modelling were the sample's coating preparation type and its thickness, the exposure media (1 mM $NaNO_3$, SS, and CCM) and the pH of the solution, the zeta potential, and the time of exposure in days, as well as the chemical composition changes in post-ageing characterisation.

To proceed with the modelling steps, data were first randomly divided into training and test sets using a ratio of 0.70 : 0.30, following a stratified sampling approach considering the sample exposure media. The training subset was used each time to adjust the model parameters, whereas the test subset was not involved in model development, and it was used as an external validation set to assess the model's performance on new (previously unseen) data. Next, the *z*-score (Gaussian) normalisation method was employed to standardise the descriptors in the training set (42 samples), ensuring their equal contribution on the model. The identical normalisation parameters were applied to the descriptors in the test set (18 samples).

Two models were then built and trained on the prepared data using XGBoost[46] and *k*-nearest neighbours (*k*NN).[21] The XGBoost model was trained on a subset of the selected variables (sample coating preparation type, thickness, exposure media, and media pH) using 100 boosting rounds. The *k*NN model was trained using all the selected variables; three neighbours (k = 3) and the neighbours' inversed distances were used as weighting factors for the prediction. To truly gauge their effectiveness, both models were subjected to the test – external validation. This involved using the test set (unseen data) to evaluate the models' generalisability in real-world scenarios.

The respective accuracy statistics of the external validation are presented in Table 3 for both models. In Fig. 6A and B, the results of the Golbraikh and Tropsha[25,26] test are presented for the *k*NN and XGBoost models, respectively. To strengthen the stakeholders' confidence on the predictions, the two models were combined under a consensus scheme: the predictions of each model are averaged, so that the overall predictive accuracy is improved. In Table 3 and in Fig. 6C, the statistics of external validation and the Golbraikh and Tropsha test results for the consensus model are presented.

The consensus model demonstrates an improved predictive accuracy compared to the *k*NN and XGBoost models and also minimizes the possible biases or limitations that could be inherent in the two individual models.

Finally, the Y-randomization test[27] was performed 10 times for the *k*NN and XGBoost models: the MAE values on the test set were calculated in the range of 0.675–1.103 using the *k*NN model, and in the range of 0.895–1.383 using the XGBoost model, confirming that the predictions were not a coincidental outcome.

Table 3 External validation results for the *k*NN and XGBoost models and the consensus model

Metric	*k*NN	XGBoost	Consensus
R^2	0.895	0.848	0.898
Q_{ext}^2	0.899	0.854	0.902
MAE	0.243	0.297	0.242
RMSE	0.316	0.379	0.311

(A)

Criterion	Assessment	Result
R^2 > 0.6	PASS	R^2 = 0.932
Rcvext^2 > 0.5	PASS	Rcvext^2 = 0.899
(R^2 - R0^2)/R^2 < 0.1	PASS	(R^2 - R0^2)/R^2 = 0.022
(R^2 - R'0^2)/R^2 < 0.1	PASS	(R^2 - R'0^2)/R^2 = 0.005
abs(R0^2 - R'0^2) < 0.3	PASS	abs(R0^2 - R'0^2) = 0.016
0.85 < k < 1.15	PASS	k = 1.091
0.85 < k' < 1.15	PASS	k' = 0.903

Model Predictive

(B)

Criterion	Assessment	Result
R^2 > 0.6	PASS	R^2 = 0.884
Rcvext^2 > 0.5	PASS	Rcvext^2 = 0.854
(R^2 - R0^2)/R^2 < 0.1	PASS	(R^2 - R0^2)/R^2 = 0.064
(R^2 - R'0^2)/R^2 < 0.1	PASS	(R^2 - R'0^2)/R^2 = 0.012
abs(R0^2 - R'0^2) < 0.3	PASS	abs(R0^2 - R'0^2) = 0.046
0.85 < k < 1.15	PASS	k = 1.081
0.85 < k' < 1.15	PASS	k' = 0.9

Model Predictive

(C)

Criterion	Assessment	Result
R^2 > 0.6	PASS	R^2 = 0.947
Rcvext^2 > 0.5	PASS	Rcvext^2 = 0.902
(R^2 - R0^2)/R^2 < 0.1	PASS	(R^2 - R0^2)/R^2 = 0.039
(R^2 - R'0^2)/R^2 < 0.1	PASS	(R^2 - R'0^2)/R^2 = 0.016
abs(R0^2 - R'0^2) < 0.3	PASS	abs(R0^2 - R'0^2) = 0.022
0.85 < k < 1.15	PASS	k = 1.093
0.85 < k' < 1.15	PASS	k' = 0.901

Model Predictive

Fig. 6 (A): Golbraikh and Tropsha test results for the *k*NN model. (B) Golbraikh and Tropsha test results for the XGBoost model, and (C) Golbraikh and Tropsha test results for the consensus model.

Applicability domain. The AD has been finally defined to establish the area of reliable predictions. For the *k*NN model, the thr value has been calculated to be equal to 1.821 based on the training samples considering only the numerical descriptors. All test samples had distance values in the range of 0–0.234, placing them within the AD limits, making their predictions reliable. Similarly, for the XGBoost model, the thr value has been calculated to be equal to 0.752 also using only numerical descriptors. The test set distance values fell in the range of 0–0.173 and thus, their predictions were considered reliable.

The *in silico* assessment of the Ni-ion release in different media can greatly support the interpretation of the experimental findings and can contribute to the strategic Safe and Sustaianble by Design (SSbD) of Ni–SiC nanocomposite electroplated coatings. In detail, the modelling results corroborate the experimental results in terms of selected variables that can effectively quantify the trends in Ni-ion release, especially the correlation to the exposure conditions (media type and pH) that influence the Ni-ion release (Ni release is highest in biological media like SS and CCM, where acidity and the presence of organic acids facilitate Ni release). Nonetheless, the models – validated with a test set – proved that the predictions closely align with the experimentally measured release values and can be generalised, providing a basis for assessing Ni-ion release in other scenarios (*e.g.*, longer exposure duration) and media not directly tested. In particular, the definition of the AD of the models allows stakeholders to strengthen their confidence on the predictions, during the models' practical use in the SSbD framework. Experimental data alone would require continuous testing under each new condition, while the models can extrapolate reliably within their applicability domain. The *in silico* approaches are a valuable cost-effective tool within the SSbD framework and their combination with the experimental assessment could also contribute to the prediction of the potentially harmful effects of Ni–SiC nanocomposite electroplated coatings.

4. Outlook

This study provides a comprehensive analysis of Ni–SiC nanocomposite coatings as a potential alternative to traditional chromium electroplating, focusing on their performance, transformation in various media, and cytotoxicity. Our findings indicate that while Ni–SiC nanocomposite coatings exhibit higher hardness and increased performance characteristics, they also present significant challenges in terms of Ni ion release and associated cytotoxicity. The enhanced Ni release, especially in biological media such as SS and CCM, highlights the potential health risks associated with these coatings. The presence of SiC NPs, although beneficial in increasing hardness, appears to exacerbate Ni release, leading to greater cytotoxic effects on MRC-5 cells compared to standalone Ni coatings.

The study also underscores the stability of SiC NPs in various media, maintaining their chemical integrity and displaying minimal dissolution. These behaviours can be attributed to their high solvation energy and low dissolution tendency, which is consistent with the existing literature. However, the increased Ni ion release from Ni–SiC nanocomposite coatings, resulting in oxidative stress and DNA damage, underscores the need for careful consideration of these materials' biological impacts.

To optimise the performance, safety, and sustainability of Ni–SiC nanocomposite coatings, several practical strategies can be applied. First, achieving uniform distribution of SiC nanoparticles within the Ni matrix is essential for maximising hardness, wear resistance, and overall durability. This can be accomplished by adjusting SiC concentrations in the electroplating bath and using ultrasonic dispersion techniques during deposition. Post-deposition treatments, such as top coating or surface polishing, can further enhance coating stability by sealing micro-pores and reducing Ni ion and SiC particle release in aggressive environments, such as synthetic sweat or cell culture media. Leveraging *in silico* modelling to predict Ni ion release in various media also supports optimising formulations, helping to meet safe by design standards by minimising environmental and health risks. Exploring multifunctional properties, such as magnetic behaviour or

radiation shielding, could extend the applications of Ni–SiC coatings, similar to tungsten-based nanocomposites used in radiation shielding while maintaining structural integrity.[9] Finally, substituting eco-friendly binders or additives in the electroplating bath supports green chemistry goals and aligns with current regulatory standards for safer industrial materials, ultimately promoting sustainable practices within the electroplating industry.

The outlook for future research includes the development of enhanced coating formulations that mitigate Ni release while preserving or improving mechanical properties. The computational models developed for predicting Ni ion release demonstrate significant potential for supporting SbD approaches in developing these coatings. Future work should also explore alternative nanoparticle materials that can offer similar mechanical benefits without the associated toxicity. Additionally, long-term studies on environmental impacts and more in-depth biological assessments will be critical for understanding and mitigating the risks associated with Ni–SiC nanocomposite coatings. This research lays a foundation for advancing the electroplating industry towards safer and more sustainable practices.

Data availability

Data will be made available by the authors upon request.

Conflicts of interest

There are no conflicts to declare.

Acknowledgements

All authors acknowledge the support from the European Union's Horizon 2020 research and innovation program (SABYDOMA Project under Grant Agreement No. 862296). We acknowledge support from the Henry Royce Institute (EPSRC grants: EP/P022464/1, EP/R00661X/1), which funded the VXSF Facilities (**https://engineering.leeds.ac.uk/vxsf**) within the Bragg Centre for Materials Research at Leeds. SC acknowledges the Engineering and Physical Sciences Research Council Co-Fund [grant number EP/X525662/1] and the NERC Independent Research Fellowship (UKRI – UKRI187), and EVJ and SC acknowledge Horizon Europe UKRI Guarantee MOZART (GA-101058450) for supporting this work.

References

1 E. Carneiro, J. D. Castro, S. M. Marques, A. Cavaleiro and S. Carvalho, REACH regulation challenge: Development of alternative coatings to hexavalent chromium for minting applications, *Surf. Coat. Technol.*, 2021, **418**, 127271.
2 K. P. Sedlazeck, *et al.*, Impact of an in-situ Cr(VI)-contaminated site remediation on the groundwater, *Environ. Sci. Pollut. Res.*, 2020, **27**(13), 14465–14475.
3 O. V. Safonova, *et al.*, Chemical composition and structural transformations of amorphous chromium coatings electrodeposited from Cr(III) electrolytes, *Electrochim. Acta*, 2010, **56**(1), 145–153.
4 M. H. Sohi, A. A. Kashi and S. M. M. Hadavi, Comparative tribological study of hard and crack-free electrodeposited chromium coatings, *J. Mater. Process. Technol.*, 2003, **138**(1–3), 219–222.
5 K. H. Hou, *et al.*, The wear behaviour of electro-codeposited Ni–SiC composites, *Wear*, 2002, **253**(9–10), 994–1003.
6 D. I. Tishkevich, *et al.*, Heavy alloy based on tungsten and bismuth: fabrication, crystal structure, morphology, and shielding efficiency against gamma-radiation, *RSC Adv.*, 2023, **13**(35), 24491–24498.
7 D. I. Tishkevich, A. I. Vorobjova, A. A. Bondaruk, E. S. Dashkevich, D. L. Shimanovich, I. U. Razanau, T. I. Zubar, D. V. Yakimchuk, M. G. Dong, M. I. Sayyed and H. H. Somaily, The Interrelation of Synthesis Conditions and Wettability Properties of the Porous Anodic Alumina Membranes, *Nanomaterials*, 2022, **12**(14), 2382.
8 P. Singh, S. W. Ali and R. D. Kale, Antimicrobial Nanomaterials as Advanced Coatings for Self-Sanitizing of Textile Clothing and Personal Protective Equipment, *ACS Omega*, 2023, **8**(9), 8159–8171.
9 A. A. Rotkovich, *et al.*, Development and study of lightweight recycled composite materials based on linear low-density polyethylene and W for radiation application, *J. Mater. Res. Technol.*, 2024, **30**, 1310–1318.
10 A. I. Vorobjova, D. I. Tishkevich, E. A. Outkina, D. L. Shimanovich, I. U. Razanau, T. I. Zubar, A. A. Bondaruk, E. K. Zheleznova, M. Dong, D. A. Aloraini and M. I. Sayyed, A study of Ta2O5 nanopillars with Ni tips prepared by porous anodic alumina through-mask anodization, *Nanomaterials*, 2022, **12**(8), 1344.
11 Y. Yao, *et al.*, Structure and shielding properties of the unsupported Bi films electrodeposited in galvanostatic and pulse regimes, *Ceram. Int.*, 2024, **50**(9), 16181–16189.
12 M. R. Vaezi, S. K. Sadrnezhaad and L. Nikzad, Electrodeposition of Ni–SiC nano-composite coatings and evaluation of wear and corrosion resistance and electroplating characteristics, *Colloids Surf., A*, 2008, **315**(1–3), 176–182.
13 J. R. A. Pires, C. Rodrigues, I. Coelhoso, A. L. Fernando and V. G. L. Souza, Current Applications of Bionanocomposites in Food Processing and Packaging, *Polymers*, 2023, **15**(10), 2336.
14 W. Begum, *et al.*, A comprehensive review on the sources, essentiality and toxicological profile of nickel, *RSC Adv.*, 2022, **12**(15), 9139–9153.
15 H. K. Bayabil, F. T. Teshome and Y. C. Li, Emerging Contaminants in Soil and Water, *Front. Environ. Sci.*, 2022, **10**, 873499.
16 S. Chakraborty, *et al.*, Does the doping strategy of ferrite nanoparticles create a correlation between reactivity and toxicity?, *Environ. Sci.: Nano*, 2023, **10**(6), 1553–1569.
17 M. Arakelyan, G. Spagnuolo, F. Iaculli, N. Dikopova, A. Antoshin, P. Timashev and A. Turkina, Minimization of Adverse Effects Associated with Dental Alloys, *Materials*, 2022, **15**(21), 7476.

18 M. R. Berthold, *et al.*, KNIME - the Konstanz information miner, *ACM SIGKDD Explorations Newsletter*, 2009, vol. 11, 1, pp. 26–31.
19 G. Melagraki and A. Afantitis, Enalos KNIME nodes: Exploring corrosion inhibition of steel in acidic medium, *Chemom. Intell. Lab. Syst.*, 2013, **123**, 9–14.
20 D. D. Varsou, *et al.*, In silico assessment of nanoparticle toxicity powered by the Enalos Cloud Platform: Integrating automated machine learning and synthetic data for enhanced nanosafety evaluation, *Comput. Struct. Biotechnol. J.*, 2024, **25**, 47–60.
21 D. D. Varsou, *et al.*, Zeta-Potential Read-Across Model Utilizing Nanodescriptors Extracted via the NanoXtract Image Analysis Tool Available on the Enalos Nanoinformatics Cloud Platform, *Small*, 2020, **16**(21), e1906588.
22 D. D. Varsou, P. D. Kolokathis, M. Antoniou, N. K. Sidiropoulos, A. Tsoumanis, A. G. Papadiamantis, G. Melagraki, I. Lynch and A. Afantitis, In silico assessment of nanoparticle toxicity powered by the Enalos Cloud Platform: Integrating automated machine learning and synthetic data for enhanced nanosafety evaluation, *Comput. Struct. Biotechnol. J.*, 2024, **25**, 47–60.
23 Y. Kang, M. G. Kim and K.-M. Lim, Machine-learning based prediction models for assessing skin irritation and corrosion potential of liquid chemicals using physicochemical properties by XGBoost, *Toxicol. Res.*, 2023, **39**(2), 295–305.
24 9789264085442-en.pdf.
25 D. L. J. Alexander, A. Tropsha and D. A. Winkler, Beware of R2: Simple, Unambiguous Assessment of the Prediction Accuracy of QSAR and QSPR Models, *J. Chem. Inf. Model.*, 2015, **55**(7), 1316–1322.
26 A. Golbraikh and A. Tropsha, Beware of q2!, *J. Mol. Graphics Modell.*, 2002, **20**(4), 269–276.
27 D. D. Varsou, *et al.*, Ecotoxicological read-across models for predicting acute toxicity of freshly dispersed versus medium-aged NMs to Daphnia magna, *Chemosphere*, 2021, **285**, 131452.
28 G. Melagraki and A. Afantitis, A Risk Assessment Tool for the Virtual Screening of Metal Oxide Nanoparticles through Enalos InSilicoNano Platform, *Curr. Top. Med. Chem.*, 2015, **15**(18), 1827–1836.
29 A. Tropsha, Best Practices for QSAR Model Development, Validation, and Exploitation, *Mol. Inf.*, 2010, **29**(6–7), 476–488.
30 D.-D. Varsou, *et al.*, A safe-by-design tool for functionalised nanomaterials through the Enalos Nanoinformatics Cloud platform, *Nanoscale Adv.*, 2019, **1**(2), 706–718.
31 Novamechanics, Welcome to Enalos+Enalos.PNG KNIME nodes, 2022 30 October, 2024, available from: **https://www.enalosplus.novamechanics.com/index.php/enalosplusnodes/**.
32 D. C. Hansen, Metal Corrosion in the Human Body: The Ultimate Bio-Corrosion Scenario, *Electrochem. Soc. Interface*, 2008, **17**(2), 31–34.
33 N. Fairley, V. Fernandez, M. Richard-Plouet, C. Guillot-Deudon, J. Walton, E. Smith, D. Flahaut, M. Greiner, M. Biesinger, S. Tougaard and D. Morgan, Systematic and collaborative approach to problem solving using X-ray photoelectron spectroscopy, *Appl. Surf. Sci. Adv.*, 2021, **5**, 100112.
34 M. C. Biesinger, *et al.*, X-ray photoelectron spectroscopic chemical state quantification of mixed nickel metal, oxide and hydroxide systems, *Surf. Interface Anal.*, 2009, **41**(4), 324–332.
35 M. C. Biesinger, *et al.*, Resolving surface chemical states in XPS analysis of first row transition metals, oxides and hydroxides: Cr, Mn, Fe, Co and Ni, *Appl. Surf. Sci.*, 2011, **257**(7), 2717–2730.
36 S. Gruber and A. Nickel, Toxic or not toxic? The specifications of the standard ISO 10993-5 are not explicit enough to yield comparable results in the cytotoxicity assessment of an identical medical device, *Front. Med. Technol.*, 2023, **5**, 1195529.
37 S. Chakraborty, *et al.*, CuO Nanoparticles as Copper-Ion Reservoirs for Elesclomol-Mediated Intracellular Oxidative Stress: Implications for Anticancer Therapies, *ACS Appl. Nano Mater.*, 2022, **5**(1), 1607–1620.
38 B. Ibrahim, *et al.*, Functionalized Gold Nanoparticles Suppress the Proliferation of Human Lung Alveolar Adenocarcinoma Cells by Deubiquitinating Enzymes Inhibition, *ACS Omega*, 2023, **8**(43), 40622–40638.
39 B. Ibrahim, T. H. Akere, S. Chakraborty, E. Valsami-Jones and H. Ali-Boucetta, Modulation of Heat Shock Protein Expression in Alveolar Adenocarcinoma Cells through Gold Nanoparticles and Cisplatin Treatment, *Pharmaceutics*, 2024, **16**(3), 380.
40 A. Kosiha, C. Parthiban and K. P. Elango, Synthesis, characterization and DNA binding/cleavage, protein binding and cytotoxicity studies of Co(II), Ni(II), Cu(II) and Zn(II) complexes of aminonaphthoquinone, *J. Photochem. Photobiol., B*, 2017, **168**, 165–174.
41 D. Schaumlöffel, Nickel species: Analysis and toxic effects, *J. Trace Elem. Med. Biol.*, 2012, **26**(1), 1–6.
42 S. Chakraborty, A. Nair, M. Paliwal, A. Dybowska and S. K. Misra, Exposure media a critical factor for controlling dissolution of CuO nanoparticles, *J. Nanopart. Res.*, 2018, **20**, 1–14.
43 B. Ibrahim, T. H. Akere, S. Chakraborty, E. Valsami-Jones and H. Ali-Boucetta, Gold Nanoparticles Induced Size Dependent Cytotoxicity on Human Alveolar Adenocarcinoma Cells by Inhibiting the Ubiquitin Proteasome System, *Pharmaceutics*, 2023, **15**(2), 432.
44 S. Barillet, *et al.*, In vitro evaluation of SiC nanoparticles impact on A549 pulmonary cells: cyto-, genotoxicity and oxidative stress, *Toxicol. Lett.*, 2010, **198**(3), 324–330.
45 A. Cacchioli, *et al.*, Cytocompatibility and cellular internalization mechanisms of SiC/SiO2 nanowires, *Nano Lett.*, 2014, **14**(8), 4368–4375.
46 D. Tarwidi, *et al.*, An optimized XGBoost-based machine learning method for predicting wave run-up on a sloping beach, *MethodsX*, 2023, **10**, 102119.

